SAND2013-10378C

INFLUENCE OF TEMPERATURE AND RESONANCE-STABILIZATION ON THE *ortho*- EFFECT IN CYMENE OXIDATION

B. Rotavera, A. M. Scheer, H. Huang, D. L. Osborn, and C. A. Taatjes*
Chemistry Department, Combustion Research Facility
Sandia National Laboratories
Livermore, CA, 94551, USA

Conference ID: CI2014

Short running title: Low-temperature autoignition chemistry of cymenes

Colloquium: Reaction Kinetics
(Alternative Colloquium): IC Engine and Gas Turbine Combustion

Total Length (Method 1):

Word Count:

- **Main Text:**
- **References:** (49 + 2) * 2.3 * 7.6
- **Equations:** (2 + 2) * 7.6 * 1
- **Fig. 1:** (30.5 + 10) * 2.2(2) + 10
- **Fig. 2:** (49.3 + 10) * 2.2(1) + 54
- **Fig. 3:** (49.3 + 10) * 2.2(1) + 21
- **Fig. 4:** (49.3 + 10) * 2.2(1) + 18
- **Fig. 5:** (49.3 + 10) * 2.2(1) + 18
- **Fig. 6:** (49.3 + 10) * 2.2(1) + 15
- **Fig. 7:** (49.3 + 10) * 2.2(1) + 15
- **Fig. 8:** (49.3 + 10) * 2.2(1) + 18
- **Fig. 9:** (49.3 + 10) * 2.2(1) + 18
- **Fig. 10:** (49.3 + 10) * 2.2(1) + 23
- **Fig. 11:** (49.3 + 10) * 2.2(1) + 23

- **Table 1:** (4 + 2) * (7.6) * (1) + 19
- **Table 1:** (4 + 2) * (7.6) * (2) + 20
- **Table 1:** (5 + 2) * (7.6) * (2) + 9
- **Table 1:** (5 + 2) * (7.6) * (2) + 4

Total:
Maximum: 5800

*Corresponding author. Sandia National Laboratories, Chemistry Department, Combustion Research Facility, Livermore, CA, 94551, USA Tel: (925) 294-2034; Email: CATaatj@Sandia.gov.

Abstract

Cymenes are monoterpenes composed of a benzene ring with *iso*-propyl and methyl substituents, and the proximity of the two alkyl groups enables relevant analysis into the *ortho*- effect of polysubstituted aromatics. The effects of substituent proximity on the initial steps of RO_2-related reactions from Cl-initiated oxidation of *ortho*-, *meta*-, and *para*-cymene were studied at low pressure (8 torr) over the temperature range 450 K – 750 K using multiplexed photoionization mass spectrometry (MPIMS). The main results are two-fold:

(i) Temperature-dependent trends of the mass spectra revealed significant chain-propagation (marked by cyclic ether yields) below 700 K only in *o*-cymene oxidation, a consequence of the *ortho*- effect; above 700 K the chain-propagation trends of the three cymenes converge.

(ii) The competition between chain-propagation channels stemming from resonance- and non-resonance-stabilized initial cymene radicals changes significantly with temperature, as evidenced experimentally in photoionization spectra and computationally using CBS-QB3-level stationary point calculations on the R + O_2 surface.

Ratios of cyclic ether formation (related to chain-propagation and OH formation) relative to HO_2-loss (related to chain-termination) were measured as a function of temperature in order to quantitatively define the *ortho*- effect. On a scale normalized to unity, over the range of temperature herein the ratio in *m*- and *p*-cymene oxidation is < 0.05, indicating minimal chain-propagation. In stark contrast, *o*-cymene exhibits significant cyclic ether formation, due to the proximity of the alkyl substituents permitting facile 6- and 7-membered-ring transition states in the formation of hydroperoxyalkyl (QOOH) intermediates from alkylperoxy radicals (ROO). The cyclic ether/HO_2-loss ratio in *o*-cymene oxidation is defined as unity at 450 K and decreases to ~ 0.10 at 700 K. The ratio for the three cymenes converges at 700 K, indicating an upper limit of temperature for the *ortho*- effect. Within the temperature region of significant chain-propagation, the experimental results of *o*-cymene oxidation indicate a competition between resonance- and non-resonance-stabilized initial radicals at lower temperature, yet with increasing temperature chain-propagation stems solely from non-resonance-stabilized initial radicals due to the back-dissociation of ROO to R + O_2 reactants, when R is resonance-stabilized. The results obtained herein for cymenes are more broadly related to the initial oxidation steps of polysubstituted aromatics with resonance- and non-resonance-stabilized radicals.

Keywords: *Cymenes, monoterpene biofuel, low-temperature oxidation, ortho- effect, resonance-stabilized radicals, chain-propagation*

1. Introduction

Practical, petroleum-derived hydrocarbon fuels for spark-ignition applications contain 10% – 45% aromatic content by volume, with monosubstituted aromatics toluene and ethylbenzene being the most abundant [1-3]. The range of aromatic fuel content for compression-ignition applications is similar, 15% – 40% [4, 5], yet is composed largely of polysubstituted aromatics [6], including dialkylbenzene species. Cymenes are dialkylbenzene terpene biofuels consisting of a benzene ring with methyl and *iso*-propyl substituents, with three isomeric configurations: *ortho*-, *meta*-, and *para*-cymene. Resulting from the identification of biosynthetic pathways [7, 8] and natural production mechanisms in plants including tobacco [9], hydrogenation of terpene-based species is of interest for generating renewable biofuels. Aside from the target species, the hydrogenation process can lead to byproducts from molecular rearrangement reactions [10]. Conversion of limonene (4-*iso*-propenyl-1-methyl-1-cyclohexene), which is a monoterpene derived from bio-oil [11], to saturated form (limonane) yields *m*-cymene (1-*iso*-propyl-3-methylbenzene) as a byproduct formed by methyl shifting during hydrogenation [12]. Varying the hydrogenation method results in specific distributions of non-aliphatic species resulting from incomplete hydrogenation or functional group-shifting from molecular rearrangement reactions [10], making possible the formation of the three cymene isomers in the case of limonene hydrogenation.

Aromatics are generally associated with decreased low-temperature reactivity compared with aliphatic species of similar carbon number. Given the reliance of low-temperature reactivity on alkylperoxy (ROO) formation and decomposition, the decrease in reactivity is ascribed partly to the lower stability of peroxy adducts from the initial R + O_2 reaction step when R is resonance-stabilized and, in the case of monoaromatics, partly to the abundance of phenylic hydrogen around the carbon ring. Phenylic C–H bond dissociation energies are ~ 15 kcal/mol higher than aliphatic analogs. Polysubstituted aromatics can alter low-temperature reactivity by enabling chain-branching pathways not present in monosubstituted aromatics. The degree of low-temperature reactivity of polysubstituted aromatics is controlled by the proximity, size, and structure of the side-chains. More specifically, of the three isomeric configurations of disubstituted benzenes, *ortho*- isomers generally exhibit a greater degree of low-temperature reactivity than *meta*- and *para*- isomers [13-16]. The increased reactivity with substituents in the *ortho*- configuration forms the basis of the *ortho*- effect which, due to facile transition states and lower-energy hydrogen-abstraction sites, enables chain-branching pathways not present in *meta*-

and *para*- isomers. Observation of *ortho*- effects were first reported in the experimental works of Salooja [13] and Barnard and Sankey [14].

Substituent effects in aromatics were studied in high-pressure shock tube and rapid compression machine ignition delay time experiments [15, 16]. Shen and Oehlschlaeger conducted high-temperature (> 1000 K) shock-tube ignition experiments from 10 – 45 atm on xylene isomers and ethylbenzene at both lean and stoichiometric equivalence ratios [15]. For temperatures above ca. 1250 K, ignition delay times were indistinguishable among the xylene isomers, yet o-xylene deviated from the trend of m- and p-xylene towards lower temperature. Ethylbenzene ignition times were consistently shorter compared to the xylenes, presumably due to the presence of benzylic C–C bond on the alkyl side-chain. The similarity of ignition delay times in the xylene trends above 1250 K is expected due to the chain-branching mechanism at higher temperatures being primarily $H + O_2 \rightarrow OH + O$ and not reliant on O_2-addition to radicals of the parent fuel, however the difference in xylene-isomer ignition towards lower temperature is attributed to the *ortho*- effect. Roubaud et al. [16] conducted low-temperature autoignition experiments near 15-atm on two *ortho*- aromatics (o-xylene and o-ethyltoluene) and n-butylbenzene using a rapid compression machine. n-butylbenzene, exhibited the strongest first-stage ignition behavior, evidenced in pressure-time histories and light emission, and the shortest second-stage ignition times. Ignition trends for o-xylene and o-ethyltoluene were similar from 650 – 725 K, yet differed markedly over the range 725 – 825 K. Roubaud et al. observed higher reactivity of o-xylene relative to o-ethyltoluene over the 100-K temperature range and ascribed the difference to second O_2-addition reactions in which the isomerized adduct of hydroperoxyalkyl radicals (QOOH) and O_2 (HOOQ′OOH) yields a phenylic radical + 2 OH + CH_2O.

The abovementioned studies of alkyl substitution effects on disubstituted-benzene ignition illustrate a dependence of low-temperature autoignition chemistry on the *ortho*- effect. The present study quantifies the *ortho*- effect in cymene isomers (Fig. 1) as a function of temperature using direct measurements of the initial steps of RO_2-related reactions pertinent to autoignition [17, 18] and, more broadly, addresses the paucity of fundamental studies on low-temperature disubstituted benzene oxidation. The single existing study on cymene ignition characteristics utilized a fused-silica reactor to study all three cymene isomers, marking ignition by the percentage of CO in the exhaust gases, where o-cymene exhibited the shortest ignition delay time and the lowest ignition temperature [13]. In the present study, the effects of methyl position on cyclic ether and HO_2 yield from Cl-initiated $R + O_2$ reactions of cymenes were examined using

multiplexed photoionization mass spectrometry over the temperature range 450 – 750 K, where cyclic ether formation is coincident with OH yield and therefore directly linked to chain-propagation in the initial steps of low-temperature hydrocarbon oxidation, and HO_2 yield is linked to chain-termination [17]. The work herein contributes a detailed and systematic analysis into the *ortho*- effect in polysubstituted aromatics, and highlights the competition between chain-propagation channels stemming from resonance-stabilized and non-resonance-stabilized QOOH radicals.

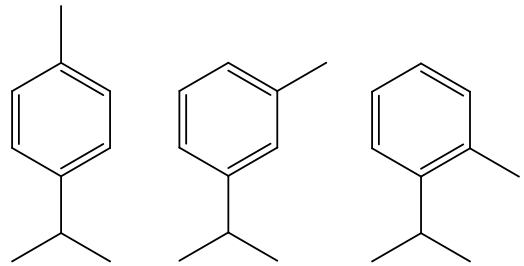

Fig. 1. Molecular structures of monoterpene (C_{10}) biofuels p-cymene, m-cymene, and o-cymene.

2. Experimental and computational approach

The experiments were performed at the Chemical Dynamics Beamline of the Advanced Light Source [19, 20] using the multiplexed photoionization mass spectrometry (MPIMS) apparatus described in Osborn et al. [21], which presently utilizes an orthogonal-acceleration time-of-flight mass spectrometer. Pulsed-photolytic chlorine atom-initiated oxidation experiments highly diluted in He were conducted using a slow-flow quartz reactor maintained at constant pressure (8 torr) over the temperature range 450 – 750 K. Flow rates during the experiments were set such that the volume inside the reactor is completely replenished between photolysis laser repetitions. To minimize side chemistry unrelated to RO_2 decomposition reactions, reactant concentrations (Table 1) employed pseudo-first-order conditions in RH + Cl and O_2 + R such that R + Cl reactions remained negligible, and the excess of O_2 over Cl_2 forces R + O_2 to be strongly favored over R + Cl_2. Fuel-depletion under the conditions in Table 1 remained near 1%.

Table 1. Pseudo-first-order experimental conditions for time history measurements during Cl-initiated oxidation of cymene isomers in Fig. 1. Approximately 1.5% of Cl_2 undergoes photolysis to generate initial Cl atoms (nominal excimer laser fluence ~ 35 mJ/cm^2). [He] was varied to maintain constant relative concentration of reactants.

Temperature (K)	450, 500, 550, 600, 650, 700, 750
Pressure (torr)	8
Cymene (molecules · cm^{-3})	$1.0 \cdot 10^{13}$
O_2 (molecules · cm^{-3})	$2.1 \cdot 10^{16}$
Cl_2 (molecules · cm^{-3})	$2.6 \cdot 10^{13}$
Cl (atoms · cm^{-3})	$3.9 \cdot 10^{11}$
He (molecules · cm^{-3})	$1.4 \cdot 10^{17}$ (450 K) – $6.8 \cdot 10^{16}$ (750 K)

Fuel-oxidation measurements were conducted over a photon energy range of 8.2 – 10.6 eV using 50-meV intervals. At fixed photon energy, photoionization mass spectra of the initial oxidation steps involving R + O_2 were recorded at 20-μs time intervals over a span of 150 ms (20-ms pre-photolysis and 130-ms post-photolysis), producing time-dependent mass spectra that were recorded sequentially at 50 discrete photon energies leading to a three-dimensional measurement (time, mass, photon energy) of the oxidation reactions. Integration of background-subtracted mass spectra at a given m/z over time and photon energy, respectively, yielded time-integrated photoionization spectra and photon energy-integrated time histories from which inference into the underlying kinetics was drawn.

Post-photolysis time histories were extracted for all three cymene isomers using the conditions in Table 1. However, since m- and p-cymene produced only negligible cyclic ether, only photoionization spectra of o-cymene oxidation were probed in detail due to the relevance to the *ortho*- effect. The mass spectra for o-cymene oxidation revealed species related to cyclic ether and HO_2-elimination channels. In order to assign isomeric contributions to mass peaks representing products of o-cymene oxidation, absolute photoionization cross-sections $\sigma(E)$ were measured in separate experiments for cyclic ether species and the HO_2-loss co-product 2-*iso*-propenyltoluene. Absolute cross-sections (Supplementary Material) were calibrated against a reference photoionization spectrum of propene from Person and Nicole [22]. Cross-sections of species herein are defined relative to the cross-section of propene at 10.325 eV (10.473 Mb) in accord with the procedure described in [23].

In order to complement the experimental results of cyclic ether measurements from the initial steps of o-cymene oxidation, stationary point energies were calculated on pathways involving decomposition of the three ROO radicals on the R + O_2 surface of o-cymene. The initial saddle point geometries and vibrational analyses were conducted using B3LYP/6-311G(d,p) within Gaussian 09 [24]. Confirmation of saddle point geometries rested on verification of single imaginary frequencies and on intrinsic reaction coordinate (IRC) calculations showing maximum energy at the coordinates of the optimized geometry. The energies of all reactants, saddle points, and products were then calculated at the CBS-QB3 level of theory. Bond dissociation energies of o-cymene were also calculated using CBS-QB3.

3. Results

Difference mass spectra (i.e. mass spectra after subtraction of pre-photolysis signals) were recorded for all three cymene isomers under the conditions in Table 1 at 10.2 eV. Except for cyclic ether peaks, which displayed a dependence on temperature, dominant mass peaks were consistent for all isomers over the range of temperatures covered and are ascribed to species formed from the reaction of interest: R + O_2. Separate experiments conducted in absence of O_2 at the highest temperature (750 K) revealed no mass peaks consistent with cymene thermal decomposition (e.g. propene). In the oxidation experiments, all isomers display a product peak at m/z 132, consistent with alkene + HO_2. However, an additional channel is strongly evident in o-cymene oxidation at temperatures below 650-K yielding a product at m/z 148. Comparison of representative time-integrated mass spectra at 500 K for the cymene isomers reveals the additional channel yielding cyclic ether which is present in the o-cymene spectrum and absent in the spectra of the other two isomers (Fig. 2). The observation of cyclic ether at 500 K only in the o-cymene spectrum is attributed to the *ortho*- effect. Similar results were obtained for other temperatures, with o-cymene oxidation yielding higher concentration of cyclic ether.

Principally, two peaks in the mass spectra are characteristic of low-temperature RO_2 decomposition pathways: HO_2-elimination, which yields an olefinic bond and accounts for the m/z 132 signal, and a concerted OH-loss/ring closure yielding cyclic ethers at m/z 148. Other common peaks in the three spectra include m/z 133, and parent depletion (m/z 134). The mass peak at m/z 133 includes ^{13}C contribution from m/z 132 and the initial R radical. However, in the o-cymene spectrum the m/z 133 is present in higher yield due to fragment ions from cyclic ether species (i.e. loss of methyl (m/z 15) from m/z 148). In all cases, parent depletion is within 1% of the initial concentration, confirming pseudo-first-order conditions.

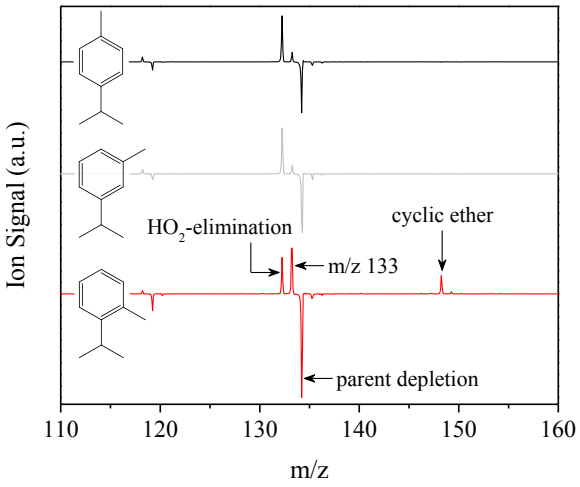

Fig. 2. Difference mass spectra of o-, m-, and p-cymene oxidation at 500 K, 8 torr, and 10.2 eV, integrated from 0 – 15 ms post-photolysis. Cyclic ether formation, observed at m/z 148, is indicative of chain-propagation and is only observed in o-cymene due to the *ortho*- effect.

Observation of the *ortho*- effect from comparison of the difference mass spectra in Fig. 2 leads to the primary focus of the present study: directly probing the effects of temperature and resonance-stabilization on initial RO_2 decomposition steps in low-temperature o-cymene oxidation. To facilitate reasoning into the initiation steps in the experiments (i.e. H-abstraction by Cl atoms), C–H bond dissociation energies were calculated at the CBS-QB3 level of theory for o-cymene. Only benzylic and primary H-abstraction sites were considered important, and the calculated energy differed substantially by approximately 10 kcal/mol (Fig. 3a). For completeness, C–H bond dissociation energies for phenylic sites were calculated, however the higher energy (ca. 113 kcal/mol) is not conducive to typical low-temperature reaction pathways. Noteworthy in Fig. 3 are the two more-facile benzylic H-abstraction sites which lead to resonance-stabilized R radicals. From subsequent O_2-addition to R radicals, alkylperoxy radicals (RO_2) create the potential for isomerization pathways to resonance-stabilized QOOH structures. For comparison, C–H bond dissociation energies were calculated for p-cymene (Fig. 3b) and are similar to the results for o-cymene.

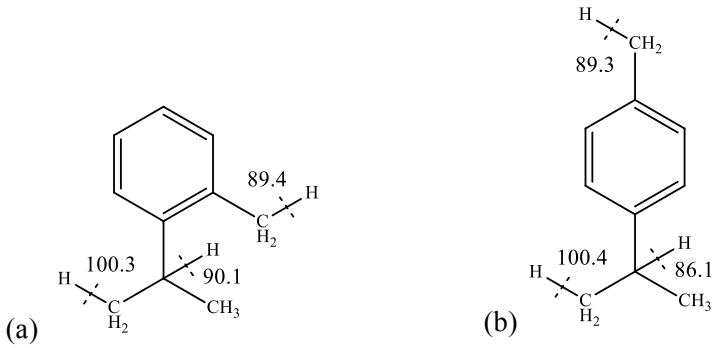

Fig. 3. CBS-QB3-calculated C–H bond dissociation energies (kcal/mol) of benzylic and primary hydrogen. (a) o-cymene; (b) p-cymene.

3.1 Effect of methyl branch location on low-temperature chain-propagation

The ratio of aggregate cyclic ether yield (m/z 148, representing chain-propagation) relative to the yield of alkene from HO_2-elimination (m/z 132, representing chain-termination) was measured for respective cymenes as a metric for the *ortho*- effect from 450 – 750 K, and was obtained using mass peaks from time-integrated ion signals measured at 10.2 eV (Fig. 4a). The temperature dependence of the ratios, depicted in Fig. 4b, indicates that below 650 K no significant cyclic ether is formed for either m- or p-cymene. In contrast, the o-cymene trend displays significant cyclic ether yield from 450 K – 650 K resulting from the additional chain-propagation pathways (i.e. the *ortho*- effect). The trend of lower cyclic ether yield with increasing temperature is indicative of the coupled effects of increased rates of HO_2-elimination and a shift towards reactants in the $R + O_2 \rightleftharpoons ROO$ equilibria. The convergence in the trends above 650 K indicates some similarity in the cymene chain-propagation mechanisms and the *ortho*- effect becoming unimportant.

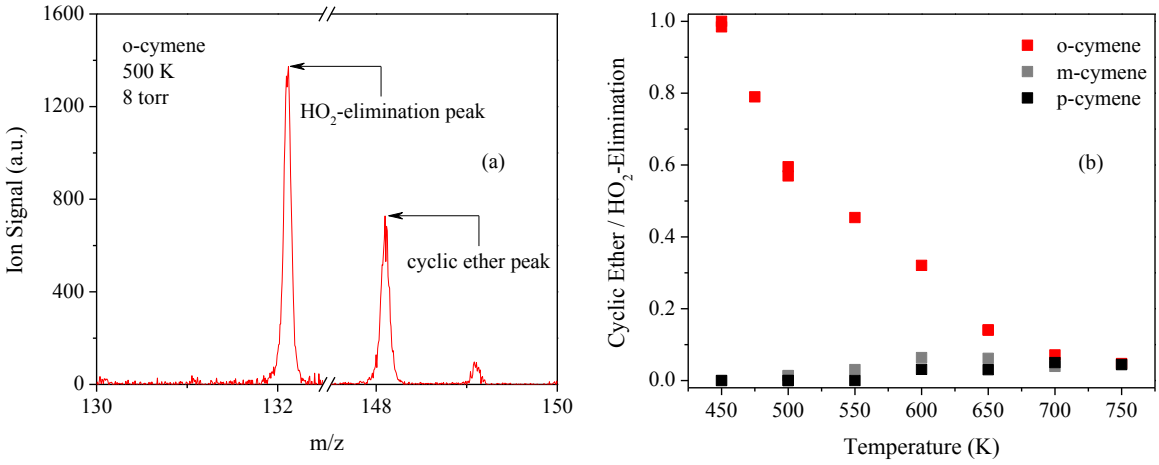

Fig. 4. (a) Representative mass peaks m/z 148 and m/z 132 from time-integrated ion signals in o-cymene oxidation at 500 K. Cyclic ether/HO_2-elimination yield ratios were defined using the m/z peaks to represent chain-propagation tendencies with temperature; the yield ratio of cyclic ether /HO_2-elimination for o-cymene at 500 K is 0.54. (b) Temperature dependence of the yield ratios in cymene oxidation quantified from 450 K – 750 K, normalized to unity. The higher ratios at lower temperatures for o-cymene is a consequence of the *ortho*- effect.

Aside from the dependence on temperature of the *ortho*- effect, Fig. 4b indicates an absence of ROO + ROO reactions forming either (i) alkoxy radicals + O_2 or (ii) ROH + RC(=O)H + O_2. Both reactions lead to species of the same m/z as cyclic ether species (m/z 148), yet since the same reaction pathways exist in both m- and p-cymene, and no m/z 148 is observed at the lower temperatures, it is inferred that RO_2 + RO_2 reactions do not contribute to product formation. Therefore, since the ratio of cyclic ether yield to HO_2-elimination is zero at the lowest temperature (450 K) where RO_2 + RO_2 reactions are most likely, contribution to m/z 148 is assigned exclusively to cyclic ether formation.

The time-dependence of cyclic ether and HO_2-elimination channels was measured at 10.2 eV (Fig. 5) and reflects the results from Fig. 4. At 500 K, no cyclic ether species are formed in m- or p-cymene oxidation. However, o-cymene oxidation exhibits significant cyclic ether formation on kinetically relevant timescales. With increasing temperature, the *ortho*- effect diminishes and all three cymene isomers exhibit similar chain-propagation kinetics: time profiles for cyclic ether formation above 650 K overlap for all three isomers. For temperatures in excess of 650 K, cyclic ether yield is ascribed exclusively to reactivity localized on the *iso*-propyl group which is the common substituent in the cymene isomers unaffected by the proximity of the methyl group. Similarly, HO_2-elimination occurs on the same substituent (*iso*-propyl) and the time profiles in Fig. 5 reflect identical time behavior for all cymene isomers.

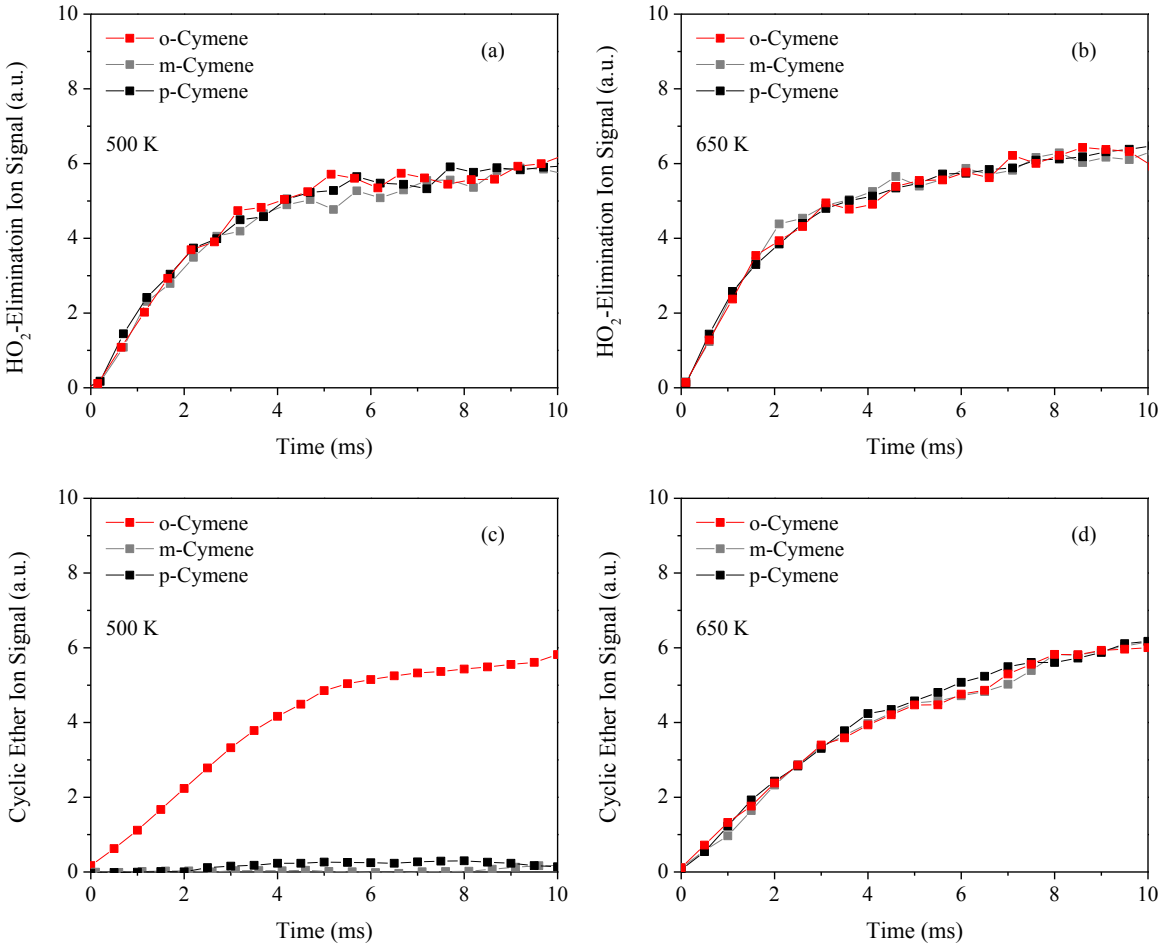

Fig. 5. Post-photolysis time histories of HO_2-elimination at (a) 550 K and (b) 650 K, and cyclic ether formation at (c) 550 K and (d) 650 K. The cymene isomers exhibit identical time behavior for HO_2-elimination for both temperatures and cyclic ether formation at 650 K, yet differ strongly in the amplitude of cyclic ether formation at 500 K due to the *ortho*- effect.

The nature of the low-temperature reactivity in o-cymene enables direct analysis of the cyclic ether channels stemming from R + O_2. Cumulatively among the three peroxy radicals of o-cymene, seven relevant cyclic ether pathways exist compared to only three cyclic ether pathways among the two peroxy radicals of m- and p-cymene (formed on the respective *iso*-propyl groups). The additional pathways in o-cymene lead to low-temperature chain-propagation and form the basis of the *ortho*- effect, namely the enabling of facile transition states across substituents which are separated by one carbon in the ring. The kinetics associated with specific chain-propagation pathways are governed partly by energy barriers along respective pathways on the R + O_2 potential energy surface, including RO_2 isomerization to QOOH and subsequent QOOH decomposition forming cyclic ether + OH. Accordingly, stationary point energy calculations reveal tendencies radical-specific tendencies.

3.2 Stationary point energy calculations

Three RO_2 radicals are relevant to the R + O_2 potential energy surface of o-cymene: one involving a non-resonance-stablized R radical (Fig. 6a) and two involving benzylic, i.e. resonance-stabilized, R radicals (Fig. 6b, 6c). Upon addition of O_2 to the benzylic radicals, the resonance stabilization is lost causing shallower ROO wells relative to well-depths associated with O_2-addition to non-resonance-stabilized R. The implications of the loss in resonance-stabilization become significant at higher temperatures, where the shallower well-depth leads to back dissociation of RO_2 towards R + O_2 [25, 26]. Stationary point energies were calculated for the pathways most relevant to auto-ignition stemming from the three RO_2 radicals: isomerization to QOOH, decomposition of QOOH to cyclic ether + OH, concerted HO_2-elimination from RO_2, and HO_2-elimination via QOOH from C–O bond scission (Figs. 7 – 9).

Two aldehyde + OH channels also exist: 2-(2-methylphenyl)propanal + OH (from radical in Fig. 6a) and 2-*iso*-propylbenzaldehyde + OH (from radical in Fig. 6b), however the CBS-QB3-calculated barrier heights for isomerization to the relevant QOOH were 14.9 kcal/mol and 17.4 kcal/mol, respectively, relative to the entrance channel of the reactants. Given the high energy, the aldehyde + OH pathways were disregarded under the conditions of the present study and the calculations focused on pathways leading to cyclic ether + OH and alkene + HO_2. The potential energy surface calculations reveal multiple low-lying pathways for o-cymene oxidation, that lead to the observed cyclic ether products at lower temperatures (cf. Fig. 4b). Moreover, the nature of o-cymene oxidation contains an inherent competition on the R + O_2 surface involving pathways from resonance- and non-resonance-stablized QOOH radicals.

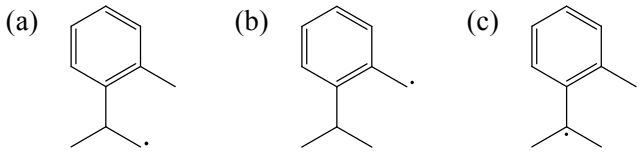

Fig. 6. Initial radicals formed by H-abstraction from o-cymene include (a) non-resonance-stabilized and (b, c) resonance-stabilized structures. Resonance effects impact the well-depth of peroxy radical adducts resulting from R + O_2 reactions and subsequent QOOH isomerzation barriers.

Addition of O_2 to the non-resonance-stablized, primary carbon of the *iso*-propyl group yields a primary alkylperoxy radical ROO(a). The resulting well-depth relative to the entrance channel is 34.5 kcal/mol (Fig. 7). Although HO_2-elimination from thermal decomposition of QOOH is possible (*QOOH(a)-3* in Fig. 7), the concerted pathway to HO_2 (i.e. from chemically activated ROO) is energetically favored, given the ~ 5 kcal/mol lower barrier to the substituted oxirane from *QOOH(a)-3*, 2-methyl-2-(2-methylphenyl)oxirane. Pathways to two other cyclic ether species are associated with ROO(a): the 6-membered cyclic ether, 3-methyl-4-benzohydropyran, and the 4-membered cyclic ether, 3-(2-methylphenyl)oxetane. Formation of the substituted oxetane (from QOOH(a)-2 in Fig. 7) is not expected to be important at lower temperature because the barrier height to QOOH decomposition is ~ 10 kcal/mol above the entrance channel. In contrast, the pathways leading to the 6- and 3-mebered cyclic ether species are important at low temperature, and are energetically competitive, particularly given the 2 – 3 kcal/mol uncertainty in CBS-QB3 calculations [27].

The two competative pathways from ROO(a) involve resonance-stabilized QOOH species. Abstraction of H from the tertiary *iso*-propyl carbon leads to resonance-stabilized *QOOH(a)–3* and abstraction of H from the methyl substituent leads to resonance-stabilized *QOOH(a)–1*. Decomposition of *QOOH(a)–3* and *QOOH(a)–1* structures lead to 3- and 6-membered cyclic ethers, respectively, and the competition between the two pathways leading to chain-propagation is inherently dependent on temperature. Notably, the difference in energy between resonance-stabilized QOOH well-depths and decomposition barriers to cyclic ether + OH is substantial. The barrier for decomposition of *QOOH(a)–1* to OH + 3-methyl-4-benzohydropyran (TS-2) is approximately 24 kcal/mol, compared with a lower-energy difference of 15 kcal/mol in the *QOOH(a)–3* case. State differently, the barrier height to QOOH decomposition leading to the 3-membered cyclic ether is approximately 9 kcal/mol lower in energy relative to the decomposition barrier to the 6-membered cyclic ether. The higher barrier to QOOH decomposition favors ROO in the ROO(a) $\rightleftharpoons$ *QOOH(a)–1* equilibrium at lower temperature, leading to competition with *QOOH(a)-3* $\rightarrow$ 2-methyl-2-(2-methylphenyl)oxirane + OH. The energetic implications alone are insufficient to select one preferential pathway since other properties of the transition state (e.g. ring strain, entropy) affect the competition. However, the lower barrier to isomerization from ROO(a) to *QOOH(a)–1* potentially favors the pathway yielding the 6-membered cyclic ether at lower temperatures.

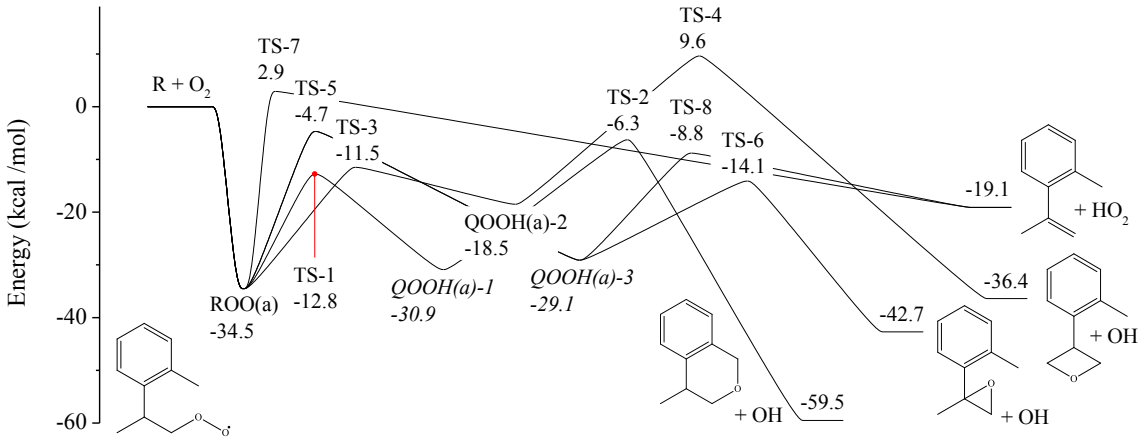

Fig. 7. CBS-QB3-calculated stationary point energies for ROO(a) decomposition reactions of the non-resonance-stabilized peroxy radical of o-cymene. Temperature induces competition between the two channels involving resonance-stabilized structures *QOOH(a)–1* and *QOOH(a)–3*.

Only two pathways exist for ROO(b) decomposition, where ROO(b) is formed from O_2-addition to the resonance-stabilized primary benzylic cymene radical. One pathway passes through a resonance-stabilzied QOOH, the other pathway through a non-resonance-stabilized QOOH (Fig. 8). The ROO(b) well-depth from O_2-addition to the resonance-stabilized R is approximately 10 kcal/mol more-shallow relative to ROO(a) (cf. Fig. 7). The effect of resonance-stabilization on ROO(b) well-depth translates to the isomerization barrier to non-resonance-stabilized QOOH (i.e. the abstracted H coming from the primary carbon of the *iso*-propyl group, QOOH(b)-1) becoming prohibitively high. Therefore, the calculations in Fig. 8 indicate that the primary peroxy radical ROO(b) preferentially passes through a resonance-stabilized QOOH structure (*QOOH(b)-2* in Fig. 8), where the abstracted H comes from the tertiary carbon of the *iso*-propyl group, and exclusively yields the 5-membered cyclic ether 2,2-dimethyl-3-benzohydrofuran + OH.

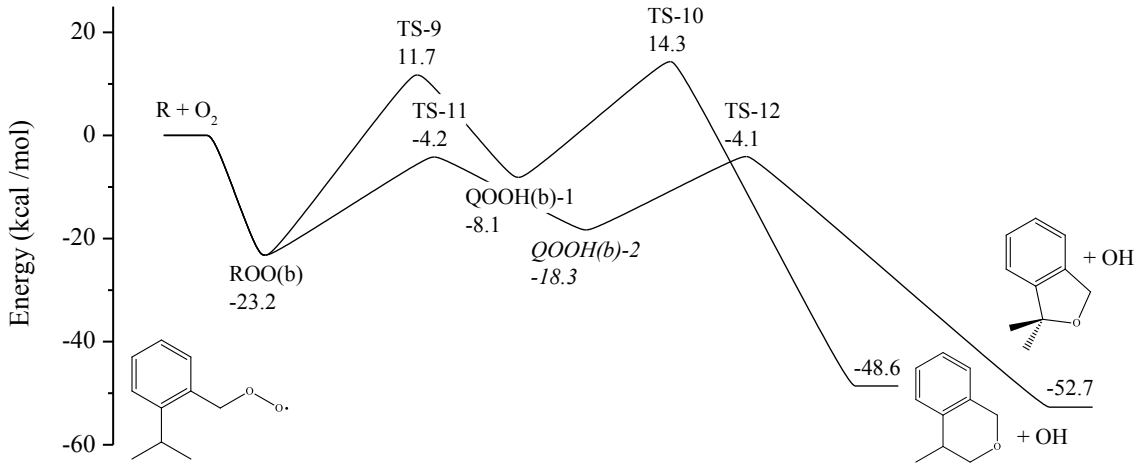

Fig. 8. CBS-QB3-calculated stationary point energies for ROO(b) decomposition reactions of the peroxy radical of o-cymene formed from O_2-addition to the resonance-stabilized primary radical. O_2-addition to the resonance-stabilized R radical favors chain-propagation via resonance-stabilized *QOOH(b)-2*.

The well-depth from O_2-addition to the tertiary benzylic site forming ROO(c) (Fig. 9) is approximately 10 kcal/mol more-shallow relative to the non-resonance-stablized well (cf. Fig. 7). The well-depth of 24.7 kcal/mol for ROO(c) is similar to that of the ROO(b) radical formed by O_2-addition to the other resonacne-stabilized radical (cf. Fig. 8). HO_2 formation from the tertiary cymene radical is highly disfavored, with the both the concerted pathway (TS-17) and thermalized pathway (TS-15) requiring energies exceeding 20 kcal/mol above the entrance channel. Chain-propagation pathways from both resonance- and non-resonance-stabilized QOOH stem from the tertiary alkylperoxy radical of o-cymene, ROO(c), leading to the 5-membered ring, 2,2-dimethyl-3-benzohydrofuran + OH and the 3-membered ring 2-methyl-2-(2-methylphenyl)oxirane + OH, respectively. The pathway leading to the substituted oxirane is energetically disfavored, with both QOOH isomerization and decomposition barriers exceeding the entrance channel. Therefore, on the basis of the stationary point energy calculations in Fig. 9, O_2-addition to the tertiary benzylic site yields only the 5-membered ring, 2,2-dimethyl-3-benzohydrofuran, formed from decomposition of the resonance-stabilized *QOOH(c)–1*.

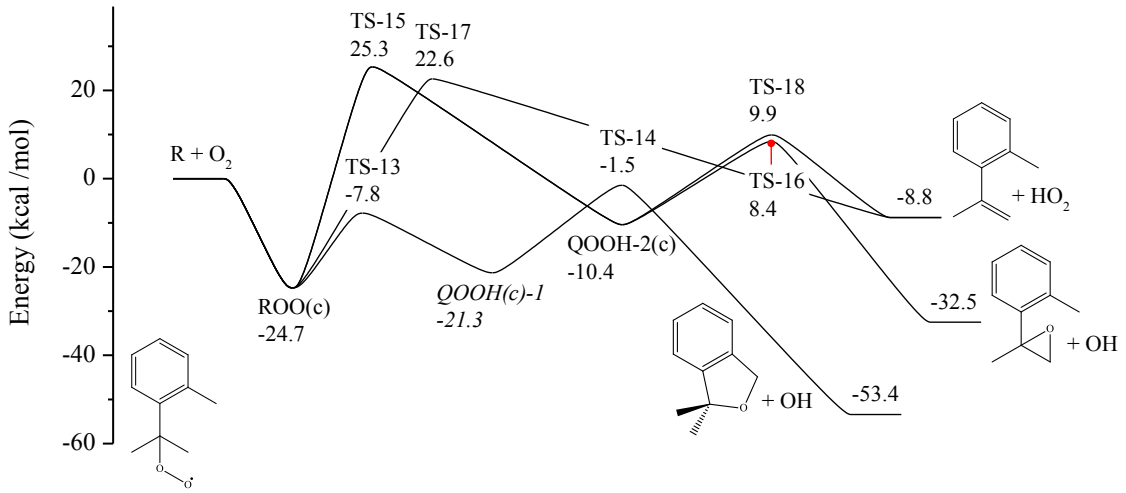

Fig. 9. CBS-QB3-calculated stationary point energies for ROO decomposition reactions of the tertiary peroxy radical of o-cymene. O_2-addition to the resonance-stabilized R radical favors chain-propagation via resonance-stabilized *QOOH(c)-1*.

3.3 Temperature dependence of chain-propagation pathways from resonance- and non-resonance-stabilized QOOH

The stationary point energy calculations indicate an effect of resonance-stabilization and temperature on the competition of cyclic ether pathways. In order to experimentally identify the variation in cyclic ether yield, temperature-dependent spectra of the cyclic ether products were measured at three temperatures: 450 K, 550 K, and 700 K. The spectra measured from oxidation experiments are compared with photoionization cross-sections of the 3- and 5-membered cyclic ether species in Fig. 10, where the cross-sections of the individual species are scaled in arbitrary units. Absent in the comparison are spectra for the 6- and 4-membered cyclic ether species (isolated samples were not available). Evidenced in the photoionization spectra in Fig. 10 is a marked dependence on temperature, reflecting varying isomeric composition.

Cyclic ether formation at 450 K (Fig. 10a) is compared to two species: 3-membered cyclic ether (2-methyl-2-(2-methylphenyl)oxirane) and 5-membered cyclic ether (2,2-dimethyl-3-beznohydrofuran). From inspection of the photoionization spectra, the ionization cross-sections of the two species appear to reproduce the trend of the cyclic ether spectrum. However, in utilizing the cross-sections of the 3- and 5-membered cyclic ethers as pseudo-basis-functions, and invoking a 2-parameter fitting routine applied to the m/z 148 spectrum, the two trends fail in reproducing the trend. The fitting result therefore indicates the presence of other cyclic ether species. Evident in Fig. 10a, however, are characteristic features attributable to the 5-membered

cyclic ether species, which is formed only from resonance-stabilized QOOH radicals (cf. Fig. 8, 9). First, the onset of the cyclic ether product photoionization spectrum occurs near 8.6 eV and matches exactly the onset energy of 5-membered heterocyclic (2,2-dimethyl-3-beznohydrofuran). Second, the two trends overlap prior to the bifurcation near 9.0 eV. Above 9.0 eV, the spectrum of the cyclic ether product appears to overlap the spectrum of the 3-membered cyclic ether, 2-methyl-2-(2-methylphenyl)oxirane, which arises exclusively from the non-resonance-stabilized cymene radical and involves a resonance-stabilized QOOH (cf. Fig. 7). However, formation of the 3-membered cyclic ether is unlikely due to the absence of any cyclic ether formation at 450 K in either m- or p-cymene oxidation. Similarly, substituted oxetane is unlikely due to the energetically disfavored barrier for QOOH decomposition to OH + cyclic ether (TS-4, Fig. 7). The remaining contributions are not immediately clear, yet the CBS-QB3-calculated adiabatic ionization energy of 3-methyl-4-benzohydropyran of 8.8 eV, in addition to the favorable energetics (cf. Fig. 7), makes the 6-membered cyclic ether most plausible. The disparity between the 2-parameter fit and the cyclic ether spectrum at 450 K is therefore likely due to the exclusion of 3-methyl-4-benzohydropyran in the fitting routine.

Increasing the temperature to 550 K resulted in a markedly different cyclic ether spectrum (Fig. 10b). The spectra of 2,2-dimethyl-3-beznohydrofuran is vertically scaled to overlap the onset energy of the cyclic ether spectrum. Qualitatively, the 5-membered cyclic ether is largely consistent with the cyclic ether spectrum, indicating significant yield at 550 K. Contribution from the 3-membered cyclic ether appears to diminish completely. Noteworthy is the 5-membered cyclic ether coming exclusively from resonance-stabilized R radicals, which indicates that for temperatures up to 550 K the $R + O_2 \rightleftharpoons ROO$ remains shifted to the product side.

The cyclic ether spectrum measured at 700 K (Fig. 10c), scaled in arbitrary units, compares favorably with the 3-membered cyclic ether. The cross-section of 2-methyl-2-(2-methylphenyl)oxirane overlaps the m/z 148 photoionization spectrum up to ~ 9.2 eV, and appears to be significant, yet does not completely define the 700-K chain-propagation channel of o-cymene. Since the m/z 148 spectrum does not display any characteristic features associated with 2,2-dimethyl-3-beznohydrofuran, the 5-membered cyclic ether is insignificant at 700 K. With increasing temperature, 2,2-dimethyl-3-beznohydrofuran becomes disfavored due to the preference for back-dissociation of ROO into $R + O_2$, where R is resonance-stabilized (cf. Fig. 8, 9). Therefore, in cymene oxidation at temperatures > 700 K, the $R + O_2 \rightleftharpoons ROO$ equilibrium for the benzylic (i.e. resonance-stabilized) radicals strongly favors the reactant side. Accordingly, the

only radical expected to contribute to cyclic ether formation is the radical on the primary carbon of the *iso*-propyl group, which leads to the 3-, 4- and 6-membered cyclic ethers (cf. Fig. 7).

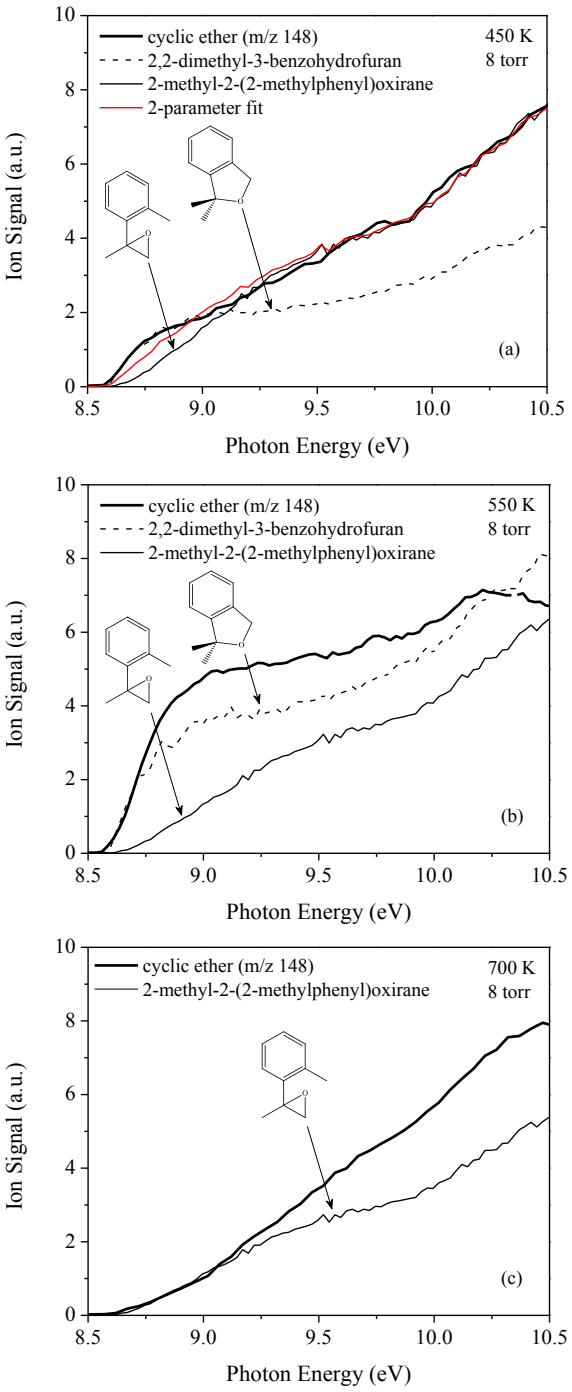

Fig. 10. Comparison of photoionization spectra of cyclic ether (m/z 148), measured during oxidation of o-cymene at (a) 450 K, (b) 550 K, and (c) 700 K, to relative photoionization cross-sections of 5- and 3-membered cyclic ether species. The variation with temperature in the cyclic ether ion signal reflects varying isomeric composition.

4. Concluding remarks

The effects of relative substituent positioning in methyl-*iso*-propyl-benzene species (i.e. cymenes) were studied experimentally from 450 – 750 K and computationally using CBS-QB3-calculated stationary point energies on the R + O_2 potential energy surface of o-cymene. Below 650 K, direct measurements of chain-propagation and chain-termination pathways revealed the temperature dependence of the *ortho*- effect in cymenes, and indicate significant chain-propagation in o-cymene oxidation, yet insignificant chain-propagation in m- and p-cymene oxidation. The *ortho*- effect diminishes with increasing temperature until 700 K, where all three cymene isomers exhibit similar chain-propagation kinetics. Lower-temperature chain-propagation is consistent with the formation of cyclic ether species from resonance- and non-resonance-stabilized initial (o-cymene) radicals, yet chain-propagation at higher temperatures arises from non-resonance-stabilized radicals. Notably, resonance-stabilized radicals contribute to chain-propagation at lower temperatures by decomposing exclusively via resonance-stabilized QOOH structures. More broadly, the results herein relate to low-temperature RO_2 reaction tendencies of polysubstituted monoaromatics with structurally inherent resonance-stabilized radicals.

References

[1] B.M. Gauthier, D.F. Davidson, R.K. Hanson, Combust. Flame, 139 (2004) 300-311.
[2] W.J. Pitz, N.P. Cernansky, F.L. Dryer, F.N. Egolfopoulos, J.T. Farrell, D.G. Friend, H. Pitsch, SAE Technical Paper 2007-01-0175, (2007).
[3] J.W. Diehl, J.W. Finkbeiner, F.P. DiSanzo, Analytical Chemistry, 67 (1995) 2015-2019.
[4] J.T. Farrell, N.P. Cernansky, F.L. Dryer, D.G. Friend, C.A. Hergart, C.K. Law, R.M. McDavid, C.J. Mueller, A.K. Patel, H. Pitsch, SAE Technical Paper 2007-01-0201, (2007).
[5] W.J. Pitz, C.J. Mueller, Prog. Energy Comb. Sci., 37 (2011) 330-350.
[6] S. Sato, Y. Sugimoto, K. Sakanishi, I. Saito, S. Yui, Fuel, 83 (2004) 1915-1927.
[7] Ryan P. McAndrew, Pamela P. Peralta-Yahya, A. DeGiovanni, Jose H. Pereira, Masood Z. Hadi, Jay D. Keasling, Paul D. Adams, Structure (London, England : 1993), 19 (2011) 1876-1884.
[8] P.P. Peralta-Yahya, F. Zhang, S.B. del Cardayre, J.D. Keasling, Nature, 488 (2012) 320-328.
[9] S. Wu, M. Schalk, A. Clark, R.B. Miles, R. Coates, J. Chappell, Nat Biotech, 24 (2006) 1441-1447.
[10] F.A. Carey, R.J. Sundberg, Advanced Organic Chemistry, 5th ed., Springer, 2008.
[11] E.E. Stashenko, R. Martínez, M.H. Pinzón, J. Ramírez, Journal of Chromatography A, 752 (1996) 217-222.
[12] N.I. Tracy, D. Chen, D.W. Crunkleton, G.L. Price, Fuel, 88 (2009) 2238-2240.
[13] K.C. Salooja, Combust. Flame, 9 (1965) 121-129.
[14] J.A. Barnard, B.M. Sankey, Combust. Flame, 12 (1968) 353-359.
[15] H.-P.S. Shen, M.A. Oehlschlaeger, Combustion and Flame, 156 (2009) 1053-1062.
[16] A. Roubaud, O. Lemaire, R. Minetti, L.R. Sochet, Combustion and Flame, 123 (2000) 561-571.
[17] J. Zádor, C.A. Taatjes, R.X. Fernandes, Progress in Energy and Combustion Science, 37 (2011) 371-421.
[18] R.W. Walker, C. Morley, Chapter 1 Basic chemistry of combustion, in: M.J. Pilling (Ed.) Comprehensive Chemical Kinetics, Elsevier, 1997, pp. 1-124.
[19] P.A. Heimann, M. Koike, C.W. Hsu, D. Blank, X.M. Yang, A.G. Suits, Y.T. Lee, M. Evans, C.Y. Ng, C. Flaim, H.A. Padmore, Review of Scientific Instruments, 68 (1997) 1945-1951.
[20] S.R. Leone, M. Ahmed, K.R. Wilson, Phys Chem Chem Phys, 12 (2010) 6564-6578.
[21] D.L. Osborn, P. Zou, H. Johnsen, C.C. Hayden, C.A. Taatjes, V.D. Knyazev, S.W. North, D.S. Peterka, M. Ahmed, S.R. Leone, Rev. Sci. Inst., 79 (2008) 104103-104110.
[22] J.C. Person, P.P. Nicole, The Journal of Chemical Physics, 53 (1970) 1767-1774.
[23] O. Welz, J. Zador, J.D. Savee, M.Y. Ng, G. Meloni, R.X. Fernandes, L. Sheps, B.A. Simmons, T.S. Lee, D.L. Osborn, C.A. Taatjes, Physical Chemistry Chemical Physics, 14 (2012) 3112-3127.
[24] M.J. Frisch, G.W. Trucks, H.B. Schlegel, G.E. Scuseria, M.A. Robb, J.R. Cheeseman, G. Scalmani, V. Barone, B. Mennucci, G.A. Petersson, H. Nakatsuji, M. Caricato, X. Li, H.P. Hratchian, A.F. Izmaylov, J. Bloino, G. Zheng, J.L. Sonnenberg, M. Hada, M. Ehara, K. Toyota, R. Fukuda, J. Hasegawa, M. Ishida, T. Nakajima, Y. Honda, O. Kitao, H. Nakai, T. Vreven, J. Montgomery, J. A., J.E. Peralta, F. Ogliaro, M. Bearpark, J.J. Heyd, E. Brothers, K.N. Kudin, V.N. Staroverov, R. Kobayashi, J. Normand, K. Raghavachari, A. Rendell, J.C. Burant, S.S. Iyengar, J. Tomasi, M. Cossi, N. Rega, J.M. Millam, M. Klene, J.E. Knox, J.B. Cross, V. Bakken, C. Adamo, J. Jaramillo, R. Gomperts, R.E. Stratmann, O. Yazyev, A.J. Austin, R. Cammi, C. Pomelli, J.W. Ochterski, R.L. Martin, K. Morokuma, V.G. Zakrzewski, G.A. Voth, P. Salvador, J.J. Dannenberg, S. Dapprich, A.D. Daniels, Ö. Farkas, J.B. Foresman, J.V. Ortiz, J. Cioslowski, D.J. Fox, (Gaussian 09, Revision A.1 Gaussian, Inc., Wallingford CT, 2009).
[25] E.W. Kaiser, T.J. Wallington, M.D. Hurley, The Journal of Physical Chemistry A, 114 (2009) 343-354.

[26] A.M. Scheer, O. Welz, J. Zádor, D.L. Osborn, C.A. Taatjes, PCCP (Submitted).
[27] J.J.A. Montgomery, M.J. Frisch, J.W. Ochterski, G.A. Petersson, The Journal of Chemical Physics, 110 (1999) 2822-2827.

Acknowledgements

The authors acknowledge financial support for the present work from the U.S-China Clean Energy Research Center (CERC) Clean Vehicle Consortium (Grant Number xyz). The Advanced Light Source is supported by the Director, Office of Science, Office of Basic Energy Sciences, of the U. S. Department of Energy under Contract DE-AC02-05CH11231 at Lawrence Berkeley National Laboratory. Sandia is a multi-program laboratory operated by Sandia Corporation, a Lockheed Martin Company, for the National Nuclear Security Administration under contract DE-AC04-94-AL85000.

Appendix A. Supplementary data

Supplemental Material I –

Supplemental Material II –

Figure captions

Figures

Table captions

Tables